

Article

A New Bi-level Optimisation Framework for Optimising a Multi-mode Wave Energy Converter Design: A Case Study for the Marettimo Island, Mediterranean Sea

Mehdi Neshat¹, Nataliia Y. Sergiienko², Erfan Amini³, Meysam Majidi Nezhad^{4*}, Davide Astiaso Garcia⁵, Bradley Alexander¹ and Markus Wagner¹

¹ Optimization and Logistics Group, School of Computer Science, The University of Adelaide, 5005 Adelaide, Australia; mehdi.neshat@adelaide.edu.au, bradley.alexander@adelaide.edu.au, markus.wagner@adelaide.edu.au

² School of Mechanical Engineering, The University of Adelaide, 5005 Adelaide, Australia; nataliia.sergiienko@adelaide.edu.au

³ Coastal and Offshore Structures Engineering Group, School of Civil Engineering, University of Tehran, 13145-1384 Tehran, Iran; erfana@ut.ac.ir

⁴ Department of Astronautics, Electrical and Energy Engineering (DIAEE), Sapienza University of Rome, 00184 Rome, Italy; meysam.majidinezhad@uniroma1.it

⁵ Department of Planning, Design and Technology of Architecture, Sapienza University of Rome, 00197 Rome, Italy; davide.astiasogarcia@uniroma1.it

* Correspondence: meysam.majidinezhad@uniroma1.it

Version April 5, 2021 submitted to Journal Not Specified

Abstract: To advance commercialisation of ocean wave energy and for the technology to become competitive with other sources of renewable energy, the cost of wave energy harvesting should be significantly reduced. The Mediterranean Sea is a region with a relatively low wave energy potential, but due to the absence of extreme waves, can be considered at the initial stage of the prototype development as a proof of concept. In this study, we focus on the optimisation of a multi-mode wave energy converter inspired by the CETO system to be tested in the west of Sicily, Italy. We develop a computationally efficient spectral-domain model that fully captures the nonlinear dynamics of a wave energy converter (WEC). We consider two different objective functions for the purpose of optimising a WEC: 1) maximise the annual average power output (with no concern for WEC cost), and 2) minimise the levelised cost of energy (LCoE). We develop a new bi-level optimisation framework to simultaneously optimise the WEC geometry, tether angles and power take-off (PTO) parameters. In the upper-level of this bi-level process, all WEC parameters are optimised using a state-of-the-art self-adaptive differential evolution method as a global optimisation technique. At the lower-level, we apply a local downhill search method to optimise the geometry and tether angles settings in two independent steps. We evaluate and compare the performance of the new bi-level optimisation framework with seven well-known evolutionary and swarm optimisation methods using the same computational budget. The simulation results demonstrate that the bi-level method converges faster than other methods to a better configuration in terms of both absorbed power and the levelised cost of energy. The optimisation results confirm that if we focus on minimising the produced energy cost at the given location, the best-found WEC dimension is that of a small WEC with a radius of 5 m and height of 2 m.

Keywords: Bi-level optimisation method; Evolutionary Algorithms; Renewable Energy, Wave Energy Converter, Geometric parameters, Power take-off, Levelised cost of energy

24 1. Introduction

25 Renewable energy is the fastest-growing new energy source globally. As an example, in the
26 United States, the growth rate of this technology increased by 100% between 2000 and 2018 [1]. On a
27 global scale, renewable energy technologies produced 26.2% of the global electricity demand in 2018,
28 and this is expected to climb to 45% by 2040 [1]. A large number of investigations have been applied
29 in order to optimise various characteristics of renewable energy systems such as dealing with the
30 uncertainty in renewable energy accessibility, support decision-making in the built environment [2]
31 and the appropriation of energy storage operations for dampening the chaotic problems [3]. Among
32 the different renewable energy sources, ocean wave energy is the cleanest, safest, most reliable and
33 predictable source of renewable energy [4] with a power density significantly higher than that of
34 solar and wind [5]. However, wave energy technology is not fully developed, and their commercial
35 penetration is still shallow. This is because the costs involved in producing energy using ocean waves
36 are currently much higher than those for other renewables [6]. Therefore, in the last decade, a large
37 number of investigations have been carried out to optimise wave energy converter (WEC) design,
38 dimensions [7–12]; power generation settings (PTO) [13,14]; and the position of WECs in a wave
39 farm [15–19].

40 The wave energy resource around the globe has been divided into six major classes depending on
41 the wave energy potential, directional and spectral characteristics, and extreme waves [20]. However,
42 it has been noted [20] that while wave energy developers mainly target wave climates with the highest
43 energy content (class 5 and 6), other resource classes can provide additional benefits to the technology
44 development. For example, the Mediterranean Sea due to its enclosed nature has low wave power
45 availability [21–23] and, belongs to the resource class 1 but the absence of extreme wave heights makes
46 this region attractive for the initial prototype testing.

47 Shape optimisation is important for all types of wave energy conversion systems, including
48 oscillating water columns [24]), and over-topping designs [25]. The majority of efforts, to date, have
49 been restricted to analysing a few specific shapes. The main reason for this is that the computational
50 demands of searching and evaluating all feasible designs are high. Vantorre et al. [26] evaluated and
51 compared the performance of a set of geometries for a heaving point absorber in a Belgian coastal
52 area. These included a hemisphere and some conical geometries. The authors proposed that the best
53 power efficiency was related to a cylindrical extension with a 90° cone. Later work by Goggins and
54 Finnegan [27] contemplated a vertical cylinder of various heights and radii under wave conditions off
55 the west coast of Ireland. They found that the most substantial significant heave velocity response was
56 that of a trimmed cylinder with a hemisphere joined to its foundation, with a whole draft to the aspect
57 ratio of 2.5. In other recent publications, a wide range of asymmetrical buoy designs has been proposed,
58 including a concave buoy face which is better able to absorb power than a flat or convex model [28].
59 Another recommendation of a surface described by bi-cubic B-spline [29] outperforms conventional
60 WEC models. However, in these studies, the main objective was to maximise the harnessed power
61 of the WEC, and the authors did not consider the design, installation and maintenance costs of these
62 asymmetric converters.

63 Other work has taken into account the trade-offs between absorbed power and the cost of building
64 and deploying the WECs. These analyses have considered the cost-efficiency or levelised cost of energy
65 (LCoE) [30]. This metric is one of the most reliable indices for the evaluation of energy investments.
66 Recently, Piscopo et al. [31] combined an LCoE minimisation with a power take-off (PTO) control
67 optimisation based on point-absorber dimensions in five Mediterranean Sea sites. This refined earlier
68 work, optimising LCoE through optimisation of both WEC geometry and PTO settings [32,33].

69 In this work, we consider a single fully submerged, three-tether, cylindrical wave energy converter.
70 This WEC is under development by Carnegie Clean Energy Limited, Australia. Two initial attempts [12,
71 34] were performed to investigate the impact of different geometries and PTO parameters on power
72 efficiency and the LCoE. However, in these prior works, only some predefined geometries were studied,
73 and the results showed that in the cylinder-shaped WEC, an optimal tethers angle depends on the

74 ratio between the buoy height and radius. However, optimisation procedures were not adequately
 75 outlined [34]. In another study [12], the performance of a few conventional optimisation methods was
 76 investigated in order to maximise the absorbed power and minimise the LCoE.

77 This paper improves upon previous research by expanding the findings of [12] to include another
 78 two state-of-the-art meta-heuristics including the Grey Wolf Optimiser [35] (GWO) and a self-adaptive
 79 version of differential evolution (LSHADE-EpSin [36]). Moreover, we propose two novel bi-level
 80 optimisation methods consisting of a global search method that works in the upper-level combined
 81 with a local search method in the lower-level. In total, nine optimisation methods are applied and
 82 compared in order to maximise the absorbed power and minimise the LCoE in a real wave regime
 83 from the southern coast of Marettimo (an island in the Mediterranean Sea). We also improve previous
 84 research by modelling waves regimes with a higher granularity of wave-directions.

85 The experimental outcomes show that a bi-level optimisation technique consisting of a
 86 self-adaptive differential evolution search (LSHADE-EpSin) interleaved with Nelder-Mead (NM)
 87 simplex direct search outperforms previous heuristic methods used in prior works in terms of
 88 convergence rate, higher absorbed power output, and lower levelised cost of energy.

89 The paper is structured as follows. Section 2 outlines the design of the WEC and the model
 90 that is applied to simulate both the absorbed power and LCoE. In the next section, the optimisation
 91 problem is described, and Section 4 represents the proposed meta-heuristic methods. The optimisation
 92 achievements are presented and considered in Section 5. Finally, section 6 presents the conclusions of
 93 this work and canvasses future work.

94 2. Modelling

95 2.1. Wave energy converter

96 A wave energy converter chosen for this case study is a fully submerged cylindrical buoy
 97 connected to three tethers to absorb wave power from its motion in multiple degrees-of-freedom
 98 (or multiple modes), namely surge, heave and pitch. As shown in Figure 1, the geometry of this WEC
 99 is determined by the radius a and height H of the cylinder, tethers inclination angle α_t , and the angle
 100 α_{ap} that defines the tether attachment point (from the centre of mass of the buoy). The submergence
 101 depth (distance from the undisturbed water level to the top of the buoy) is considered fixed and equal
 102 to 2 m regardless of the buoy size. The mass of the buoy is taken as half the displaced mass of water
 103 $m_b = 0.5\rho_w V$ (the density of water is $\rho_w = 1025 \text{ kg/m}^3$, and the buoy volume is $V = \pi a^2 H$). The
 104 hollow buoy houses three direct mechanical drive power take-off units (each connected to the tether).
 105 Each PTO acts as a spring-damper system where stiffness and damping coefficients can be adjusted for
 106 each sea state.

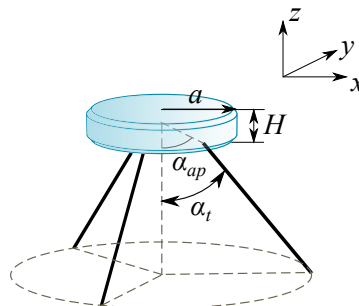


Figure 1. A three-tether wave energy converter.

107 2.2. Wave climate

108 A potential wave energy development site located near the west coast of Marretimo Island
 109 (Italy) in the Mediterranean Sea is chosen for this analysis. According to the WXSD classification

110 [20], this wave climate belongs to resource class 1 due to its low energy content (6.4 kW/m). The
 111 k-means clustering method has been applied to extract 10 sea states that represent this wave climate as
 112 shown in Figure 2 and listed in Table 1. A weighted aggregation of these 10 irregular sea states are
 113 used to calculate the annual average power production of the WEC. It is assumed that all waves are
 114 unidirectional and propagate in the positive x -direction.

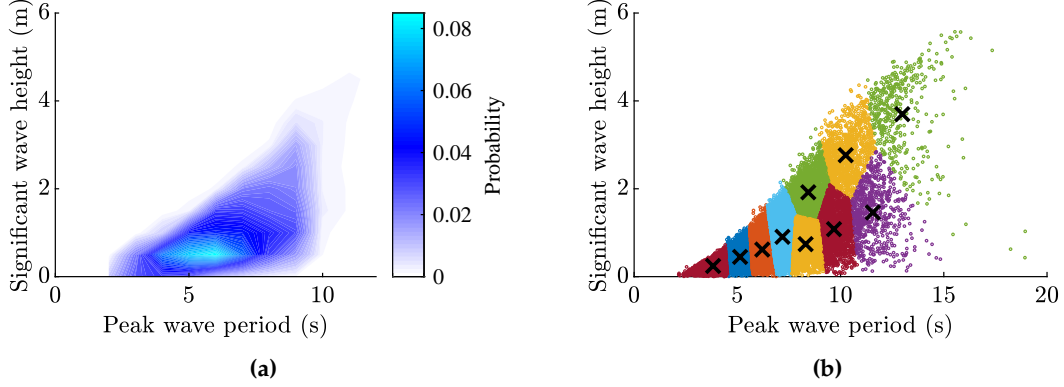


Figure 2. The wave climate at the Marettimo deployment site, Italy (12.04°E, 37.96°N, 6.38 kW/m mean annual wave power resource) [37]: (a) wave scatter diagram, and (b) clustering of the wave data where crosses correspond to ten representative states.

Table 1. 10 irregular sea states that represent the Marettimo deployment site.

Sea state	T_p, s	H_s, m	Probability $O, \%$
1	3.82	0.24	8.06
2	5.13	0.44	14.62
3	6.20	0.61	17.80
4	7.18	0.90	18.01
5	8.30	0.73	12.10
6	8.43	1.92	9.58
7	9.68	1.08	8.68
8	10.24	2.76	5.78
9	11.56	1.46	3.30
10	12.99	3.69	2.07

115 2.3. Equations of motion

The following time-domain model describes the WEC response under the wave and PTO loads:

$$\mathbf{M}\ddot{\mathbf{x}}(t) = \mathbf{F}_{exc}(t) + \mathbf{F}_{rad}(t) + \mathbf{F}_{visc}(t) + \mathbf{F}_{buoy}(t) + \mathbf{F}_{tens}(t), \quad (1)$$

116 where the $\mathbf{x} \in \mathbb{R}^{6 \times 1}$ is the buoy position vector in $Oxyz$ coordinate system, \mathbf{M} is a mass matrix, \mathbf{F}_{exc}
 117 is the wave excitation force, \mathbf{F}_{rad} is the wave radiation force, \mathbf{F}_{visc} is the viscous drag force, \mathbf{F}_{buoy} is
 118 the buoyancy force, \mathbf{F}_{tens} is the tether tension force expressed in the Cartesian space that includes the
 119 pre-tension force and control (PTO) forces. The force acting along the k -th tether can be modelled
 120 as $F_{t,k} = F_{t0} + K_{pto}\Delta\ell_k + B_{pto}\dot{\Delta\ell}_k$ ($k = 1 \dots 3$) being proportional to the tether extension $\Delta\ell$, the rate
 121 of change of the tether length $\dot{\Delta\ell}$ and includes the initial tension F_{t0} . The PTO stiffness K_{pto} and
 122 damping B_{pto} coefficients take the same values for all three tethers. The transformation between the
 123 buoy velocity $\dot{\mathbf{x}}$ and the tether velocity vector $\dot{\mathbf{q}} = [\dot{\Delta\ell}_1 \quad \dot{\Delta\ell}_2 \quad \dot{\Delta\ell}_3]^T$ has a form of $\dot{\mathbf{q}}(t) = \mathbf{J}^{-1}(\mathbf{x})\dot{\mathbf{x}}(t)$,
 124 where $\mathbf{J}^{-1}(\mathbf{x}) \in \mathbb{R}^{3 \times 6}$ is the inverse kinematic Jacobian that depends on the buoy position at each
 125 time instance [34]. So the tether force vector can be converted to the Cartesian space according to
 126 $\mathbf{F}_{tens} = -\mathbf{J}^{-T}\mathbf{F}_t$.

127 The time-domain model in Eq. (1) has a relatively high computation time and may not be
 128 suitable for optimisation purposes when a large number of evaluations are required. If to assume
 129 that all processes are Gaussian, it is possible to derive a spectral-domain model that can capture all
 130 required nonlinear forces using statistical linearisation technique [38,39]. The spectral-domain model
 131 approximates the system dynamics in the frequency domain by replacing all nonlinear terms with
 132 equivalent linear matrices [40]. The dynamic model in Eq. (1) has two sources of nonlinearity: the
 133 viscous drag force \mathbf{F}_{visc} and the generalised tether tension force \mathbf{F}_{tens} . Due to the fact that geometric
 134 nonlinearity contained within \mathbf{F}_{tens} is much weaker than the quadratic nonlinearity in \mathbf{F}_{visc} , \mathbf{F}_{tens} can
 135 be linearised around the zero position without loss of accuracy for the proposed configuration. If
 136 nonlinear effects from tethers become relevant, the equivalent terms can be derived as shown in
 137 [38,41,42]. Moreover, it should be noted that other nonlinear forces can be included in the model
 138 but omitted in this study, e.g. nonlinear Froude-Krylov force that becomes relevant when the buoy
 139 experiences large motion amplitudes [43]. As a result, a nonlinear dynamic Eq. (1) is replaced by the
 140 equivalent frequency domain model:

$$\left[-\omega^2 (\mathbf{M} + \mathbf{A}(\omega)) + i\omega (\mathbf{B}(\omega) + \mathbf{B}_{pto} + \mathbf{B}_{eq}) + \mathbf{K}_{pto} \right] \hat{\mathbf{x}}(\omega) = \hat{\mathbf{F}}_{exc}(\omega), \quad (2)$$

where $\mathbf{x}(t) = \Re\{\hat{\mathbf{x}} e^{i\omega t}\}$, the radiation force is expressed using the frequency dependent added mass $\mathbf{A}(\omega)$ and radiation damping matrix $\mathbf{B}(\omega)$, $\hat{\mathbf{F}}_{rad}(\omega) = -(-\omega^2 \mathbf{A}(\omega) + i\omega \mathbf{B}(\omega)) \hat{\mathbf{x}}(\omega)$, the tether tension force is linearised as $\hat{\mathbf{F}}_{tens}(\omega) = -(i\omega \mathbf{B}_{pto} + \mathbf{K}_{pto}) \hat{\mathbf{x}}(\omega)$ (see [44] for more details), and the viscous drag force is replaced by $\hat{\mathbf{F}}_{visc}(\omega) = -i\omega \mathbf{B}_{eq} \hat{\mathbf{x}}(\omega)$. The equivalent damping term \mathbf{B}_{eq} is unknown and determined iteratively (for each wave condition separately) using the procedure explained in [38]:

$$\mathbf{B}_{eq} = - \left\langle \frac{\partial \mathbf{F}_{visc}}{\partial \dot{\mathbf{x}}} \right\rangle, \quad (3)$$

where $\langle \cdot \rangle$ indicates mathematical expectation, and the viscous force is interpreted as:

$$\mathbf{F}_{visc} = -\frac{1}{2} \rho_w \mathbf{C}_d \mathbf{A}_d (|\dot{\mathbf{x}}| \odot \dot{\mathbf{x}}), \quad (4)$$

141 ρ_w is the density of water, \mathbf{C}_d and \mathbf{A}_d are the matrices of the drag coefficients and the cross-section areas
 142 of the buoy perpendicular to the direction of motion respectively, and \odot represents the Hadamard
 143 product (element-wise multiplication). Note that only the body velocity (not the relative fluid/body
 144 velocity) has been considered in the drag force formulation. A detailed methodology of how to
 145 incorporate the wave-particle velocity into the spectral-domain model is demonstrated in [45].

146 The following iterative procedure is used to estimate \mathbf{B}_{eq} and approximate the response of the
 147 WEC in irregular waves:

- 148 Step 1. Define the sea state and corresponding incident wave spectrum $S_\eta(\omega)$.
 Step 2. Compute the power spectral density (PSD) matrix of the excitation force:

$$\mathbf{S}_F(\omega) = S_\eta(\omega) \hat{\mathbf{f}}_{exc}(\omega) \hat{\mathbf{f}}_{exc}^*(\omega), \quad (5)$$

149 where $\hat{\mathbf{f}}_{exc}$ is the vector of excitation force coefficients, and $(\cdot)^*$ denotes the conjugate transpose
 150 of a vector/matrix.

- Step 3. Calculate the WEC response matrix assuming $\mathbf{B}_{eq} = \mathbf{0}_{6 \times 6}$ in the first iteration:

$$\mathbf{H}(\omega) = \left[-\omega^2 (\mathbf{M} + \mathbf{A}(\omega)) + i\omega (\mathbf{B}(\omega) + \mathbf{B}_{pto} + \mathbf{B}_{eq}) + \mathbf{K}_{pto} \right]^{-1}. \quad (6)$$

- Step 4. Establish the power spectral density matrix of the buoy motion:

$$\mathbf{S}_x(\omega) = \mathbf{H}(\omega) \mathbf{S}_F(\omega) \mathbf{H}^*(\omega). \quad (7)$$

Step 5. Calculate the covariance matrix of the WEC velocity:

$$\sigma_{\dot{\mathbf{x}}}^2 = \text{cov}[\dot{\mathbf{x}}, \dot{\mathbf{x}}] = \int_0^\infty \omega^2 \mathbf{S}_{\mathbf{x}}(\omega) d\omega. \quad (8)$$

Step 6. Estimate the equivalent damping matrix \mathbf{B}_{eq} using the analytical expression from [38]:

$$\mathbf{B}_{eq} = - \left\langle \frac{\partial \mathbf{F}_{visc}}{\partial \dot{\mathbf{x}}} \right\rangle = \frac{1}{2} \sqrt{\frac{8}{\pi}} \rho_w \mathbf{C}_d \mathbf{A}_d \sigma_{\dot{\mathbf{x}}}^2. \quad (9)$$

Step 7. Check the convergence criteria:

$$|\mathbf{B}_{eq}[n] - \mathbf{B}_{eq}[n-1]| < \delta. \quad (10)$$

151 where n corresponds to the iteration number, and the threshold is set to $\delta = 0.01$. If this
152 condition is not satisfied, go to Step 3.

It can take up to 10 iterations to estimate \mathbf{B}_{eq} and the WEC response in irregular waves. Once calculated, the average power absorbed by each PTO unit $k = 1 \dots 3$ is calculated as [38]:

$$\bar{P}_k = B_{pto} \sigma_{\dot{q}_k}^2, \quad (11)$$

where $\sigma_{\dot{q}_k}^2$ is the variance of the tether length rate change \dot{q} :

$$\sigma_{\dot{q}_k}^2 = \int_0^\infty \omega^2 S_{q_k}(\omega) d\omega, \quad (12)$$

153 and the transformation between the Cartesian coordinate system and the tether space is obtained
154 using $\mathbf{S}_q(\omega) = \mathbf{J}_0^{-1} \mathbf{S}_x(\omega) \mathbf{J}_0^{-T}$, where $\mathbf{J}_0^{-1} = \mathbf{J}^{-1}(\mathbf{x}_0)$ is linearised about the nominal operating position
155 $\mathbf{x}_0 = \mathbf{0}_{6 \times 1}$.

The total power generated by three PTO units in an irregular wave with the significant wave height H_s and peak wave period T_p is:

$$\bar{P}(H_s, T_p) = B_{pto} \sum_{k=1}^3 \sigma_{\dot{q}_k}^2(H_s, T_p). \quad (13)$$

The expected average annual power production from the WEC for a specific deployment site is estimated as:

$$P_{AAP} = \sum_{H_s} \sum_{T_p} \mathbf{O}(H_s, T_p) \cdot \bar{P}(H_s, T_p), \quad (14)$$

156 where the matrix $\mathbf{O}(H_s, T_p)$ contains the occurrence probability of each sea state within the wave
157 climate.

158 To demonstrate that a spectral-domain model is an effective tool that can fully capture the
159 nonlinear dynamics of the considered WEC while significantly decreasing the computation time,
160 a comparison of average power estimated using three different models is shown in Fig. 3. The
161 frequency-domain model is implemented based on Eq. (2) assuming $\mathbf{B}_{eq} = \mathbf{0}$, the spectral-domain
162 model is specified in Eq. (2) where \mathbf{B}_{eq} is estimated iteratively for each sea state, and the time-domain
163 model is represented by Eq. (1). Good agreement is achieved between the spectral-domain and
164 time-domain models, while the frequency domain model significantly overestimates power generation
165 potential of the WEC.

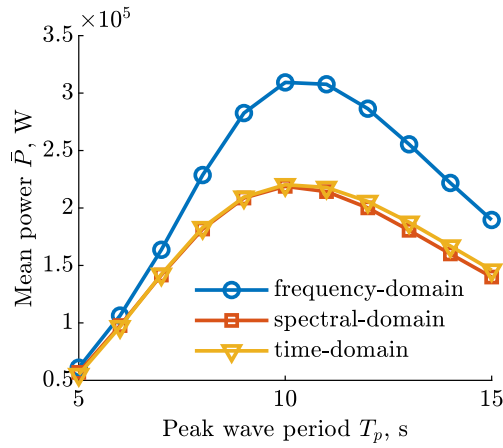


Figure 3. Power production of a three-tether WEC in irregular waves estimated using three different models: frequency-, spectral-, and time-domain. Parameters of the WEC are $a = 5.5$ m, $H = 5.5$ m, $\alpha_{ap} = \alpha_t = 45$ deg, $K_{pto} = 200$ kN/m, $B_{pto} = 150$ kN/(m/s)), irregular waves have the significant wave height of $H_s = 3$ m and modeled using the Pierson-Moskowitz spectrum.

166 2.4. Economic model

167 Levelised cost of energy (LCoE) is used to measure the economic attractiveness of the proposed
 168 energy project. Due to the lack of publicly available information of the detailed cost estimations for
 169 wave energy technology, [46] proposed to approximate LCoE by the following equation:

$$\text{LCOE} \left(\frac{\text{€}}{\text{kWh}} \right) = \text{RDC} \times \left(\frac{\text{Energy (MWh)}}{\text{Mass (kg)}} \right)^{-0.5}, \quad (15)$$

170 where RDC is a site-specific coefficient that is set to 1 in this study, the characteristic mass of the system
 171 includes the mass of the buoy and the anchoring system.

172 The characteristic mass of the WEC is calculated using the following assumptions:

- 173 - the mass of the buoy is calculated based on a given geometry as $m_b = 0.5\rho_w\pi a^2H$;
- 174 - the needed mass of the anchoring system (three piles) relays on the tether tension associated
 175 with buoyancy and the wave force, and can be approximated by $m_{as} \approx 0.116F_t^{peak}$ using case
 176 presented in [47] as a reference. The tether peak force (99% = $2.57\sigma_{F_t}$) is estimated from the
 177 spectral-domain model.

As a consequence, the LCoE model applied in this research is:

$$\text{LCOE} = \left(\frac{8760P_{AAP}}{m_b + m_{as}} \right)^{-0.5}. \quad (16)$$

178 2.5. Implementation

179 To estimate the power output and LCoE for any WEC geometry, Eq. (2) is solved in MATLAB.
 180 The mass matrix has a diagonal form $\mathbf{M} = \text{diag}(m_b, m_b, m_b, I_{xx}, I_{yy}, I_{zz})$ with moments of inertia
 181 calculated for the cylindrical body. Hydrodynamic parameters of the WEC, including the added
 182 mass $\mathbf{A}(\omega)$, hydrodynamic damping $\mathbf{B}(\omega)$, and excitation force vector $\hat{\mathbf{F}}_{exc}(\omega)$ are estimated using
 183 a semi-analytical model [48,49]. \mathbf{B}_{eq} is calculated based on the iterative procedure explained in
 184 Section 2.3.

185 Even though only one geometric shape (vertical cylinder) is used in the study, the magnitude
 186 of the viscous drag force, and the corresponding \mathbf{B}_{eq} , are highly dependent of the ratio between
 187 the cylinder height to its diameter, especially for the heave mode. Therefore, it order to develop an
 188 optimisation procedure that can accommodate WEC geometries with various aspect ratios (H/a), the

189 drag coefficient in heave is expressed as a function $C_{d_3} = -0.12(H/a) + 1.2$ based on published data
 190 [50] shown in Fig. 4. Drag coefficients in other directions are not sensitive to the cylinder aspect ratio
 191 and are kept fixed $C_{d_1} = C_{d_2} = 1$ for surge and sway, and $C_{d_4} = C_{d_5} = 0.2$ for roll and pitch. The
 192 irregular waves from Table 1 are modelled using the Bretschneider (modified Pierson-Moskowitz)
 193 spectrum according to [51].

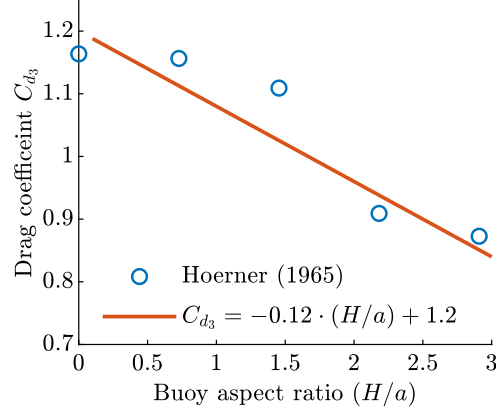


Figure 4. Drag coefficient of the cylindrical body in axial flow as a function of its aspect ratio H/a .

194 3. Optimisation Configuration Models

195 In this research, The optimisation decision variables of the cylinder are including the radius
 196 of the buoy a , the aspect ratio that is considered as the proportion of the height over the radius of
 197 the buoy (H/a), two tether angles (attachment α_{ap} and inclination angle α_t), two vectors of power
 198 take-off parameters, damping and stiffness coefficients represented $\mathbf{b}_{pto} = [B_{pto}^{(1)}, B_{pto}^{(2)}, \dots, B_{pto}^{(N)}]^T$ and
 199 $\mathbf{k}_{pto} = [K_{pto}^{(1)}, K_{pto}^{(2)}, \dots, K_{pto}^{(N)}]^T$ respectively. The length of each PTO vector is $N = 10$. The whole
 200 number of decision designs are 24 which should be optimised in the following:

$$\mathbf{z}_1 = [a, H, \alpha_t, \alpha_{ap}, \mathbf{k}_{pto} \in \mathbb{R}^{N \times 1}, \mathbf{b}_{pto} \in \mathbb{R}^{N \times 1}]. \quad (17)$$

$$\mathbf{z}_2 = [a, (H/a), \alpha_t, \alpha_{ap}, \mathbf{k}_{pto} \in \mathbb{R}^{N \times 1}, \mathbf{b}_{pto} \in \mathbb{R}^{N \times 1}]. \quad (18)$$

201 We apply two fitness functions in order to maximise the power output and minimise the LCoE.

(i) The average annual produce power output computed utilising Eq. (14), that is maximised as

$$f_{O1} = \arg \max_{\mathbf{z}} P_{AAP}(\mathbf{z}), \text{ subject to: } \mathbf{z}_1 \in [\mathbf{z}_{\min}, \mathbf{z}_{\max}] \quad (19)$$

(ii) The LCoE is minimised using the below equation that is specified in Eq. (16):

$$f_{O2} = \arg \min_{\mathbf{z}} \text{LCOE}(\mathbf{z}), \text{ subject to: } \mathbf{z}_2 \in [\mathbf{z}_{\min}, \mathbf{z}_{\max}] \quad (20)$$

202 Table 2 shows the ranges of all design variables which are involved in the optimisation process.

203 4. Optimisation Algorithms

204 In this paper, we focus on two widespread optimisation strategies in order to maximise harnessed
 205 power and minimise the levelised cost of energy (LCoE) of a fully-submerged three-tether WEC.
 206 The first approach applies optimisation algorithms to all decision variables simultaneously. These
 207 design variables consist of the buoy geometry parameters (radius a , height H and aspect ratio (H/a)),

Table 2. Boundary Constraints of the Cylinder parameters.

Parameter	Unit	Min	Max	Length
radius, a	m	1	20	1
height, H	m	1	30	1
aspect ratio, (H/a)		0.4	2	1
Tether inclination angle, α_t	deg	10	80	1
Tether attachment angle, α_{ap}	deg	10	80	1
PTO stiffness, K_{pto}	N/m	10^3	10^8	10
PTO damping, B_{pto}	N/(m/s)	10^3	10^8	10

208 the tether angles (inclination angle α_t and the tether attachment angle α_{ap}), and the PTO parameters
 209 (spring stiffness k_{pto} and damping coefficients k_{pto}). In total, there are 24 parameters that are optimised
 210 all-at-once.

211 The second strategy is to apply bi-level optimisation methods [52], which solve the problem using
 212 a two-level optimisation procedure, where one optimisation problem is nested within the other. The
 213 outer optimisation task is generally regarded as the upper-level optimisation problem, and the interior
 214 one is recognised as the lower-level optimisation problem. A significant characteristic of the bi-level
 215 optimisation problem is that the fitness functions of each level may be partly defined by variables
 216 advised by other levels. Following this strategy, we propose two bi-level optimisation methods and
 217 compare their performance with seven other well-known global search methods. The details of the
 optimisation algorithms performed for each strategy are outlined in Table 3.

Table 3. The details of the optimisation methods Settings. All approaches are restricted to the same evaluation number.

Methods	Settings
Nelder-Mead [53]	Nelder-Mead simplex direct search (NM)
1+1EA [54]	mutation step sizes are $\sigma_a = \zeta_1 \times (U_a - L_a)$, $\sigma_H = \zeta_1 \times (U_H - L_H)$, $\sigma_{\alpha_t} = \sigma_{\alpha_{ap}} = \zeta_1 \times (U_{\alpha_t} - L_{\alpha_t})$, $\sigma_{K_{pto}} = \sigma_{B_{pto}} = \zeta_2 \times (U_{K_{pto}} - L_{K_{pto}})$, and Probability mutation rate = $\frac{1}{N}$, $\zeta_1 = 0.3$, $\zeta_2 = 0.01$
CMA-ES [55]	with the default settings and $\lambda = 13$;
PSO [56]	with $\lambda = 25$, $c_1 = 1.5$, $c_2 = 2$, $\omega = 1$ (decreased with a damping ratio $w_f = 0.99$ exponentially);
GWO [35]	with $\lambda = 25$, $\alpha = 2$ (linearly decreased to zero)
DE [57]	with $\lambda = 25$, $F = 0.5$, $P_{cr} = 0.8$
SaDE [58]	with $\lambda = 25$, $LP = 50$, $NumSt = 4$
LSHADE-EpSin [36]	$\lambda = 25$, historical memory size $H = 5$, $Num_{LS} = 10$
Bi-level-1	SaDE +NM, WEC's dimensions and tether angles are optimised in the lower-level, default settings of SaDE
Bi-level-2	LSHADE-EpSin + NM, WEC's dimensions and tether angles are optimised in the lower-level, default settings of LSHADE-EpSin

218

219 4.1. All-at-Once Optimisation

220 Various factors associated with WEC design, tether angles and PTO parameters combined to form
 221 a non-convex, dynamic, constrained and large-scale optimisation problem. These challenges serve as
 222 our primary motivation for applying the meta-heuristics like evolutionary and swarm optimisation
 223 algorithms. We apply and compare the performance of seven well-known meta-heuristics that reliably
 224 optimise all decision variables of WECs all-at-once. This optimisation process leads to maximise the
 225 produced power and minimise the levelised cost of energy. The optimisation methods applied in this
 226 research include 1+1EA [59]; Differential Evolution (DE) [57], Covariance matrix adaptation evolution
 227 strategy (CMA-ES) [55], Particle Swarm Optimisation (PSO) [56], Grey Wolf Optimiser (GWO) [35] and
 228 two state-of-the-art self-adaptive optimisation methods including SaDE [58] and LSHADE-EpSin [36].

229 4.1.1. L-SHADE with an Ensemble pool of Sinusoidal Parameter Adaptation (LSHADE-EpSin)

230 The Differential Evolution (DE) algorithm, and its adaptive and self-adaptive variants, are simple
 231 and robust evolutionary algorithms. Researchers from various fields of science and engineering have
 232 applied DE algorithms to various optimisation problems, notwithstanding problems with characteristic
 233 such being continuous, multi-modal, combinatorial or mixed variable. DE is able to obtain superior
 234 optimisation results across widely encountered real-world engineering problems [60,61]. Among
 235 a wide range of self-adaptive DE algorithms, LSHADE-EpSin performs outstandingly in solving
 236 different benchmarks and real-world problems [36]. LSHADE-EpSin is a modified version of the
 237 L-SHADE algorithm [62] with linear population size reduction and an ensemble pool of sinusoidal
 238 parameter adaptations. L-SHADE is a developed version of the SHADE algorithm [63] that practices a
 239 history-based parameter adaptation trajectory based on the JADE algorithm [64] which proposed the
 240 novel mutation strategy (*current/to/pbest*).

241 Mutation Strategy with External Archive

242 In LSHADE-EpSin, one of the best-performing mutation strategies for generating promising
 243 mutant vectors during the optimisation process is *current-to-pbest/l* which is initially proposed by
 244 JADE. This mutation strategy can be seen in Equation 21.

$$\mathbf{v}_{i,g} = x_{i,g} + F_{i,g}(x_{pbest,g} - x_{i,g}) + F_{i,g}(x_{r_1,g} - x_{r_2,g}) \quad (21)$$

245 where $x_{pbest,g}$ is chosen from the best solutions $N \times p$ ($p \in [0, 1]$) of the current parent population
 246 (g). $x_{r_1,g}$ is randomly taken from the population and $x_{r_2,g}$ is randomly chosen from a combination
 247 of the current population and the external archive (A). The external archive keeps a record of the
 248 lower-ranking parents recently replaced by offspring.

249 Ensemble of Parameter Adaptation

250 An ensemble of parameter configurations is used in LSHADE-EpSin to control the adaptation of
 251 parameters. The adaptive parameters are associated with a combination of two sinusoidal formulas to
 252 adjust the scaling factor. Firstly, a non-adaptive sinusoidal adjustment technique is used to adjust the
 253 scale factor ($F_{i,g}$) which decreases during the optimisation process. Equation 22 shows this non-adaptive
 254 technique.

$$F_{i,g} = \frac{1}{2} \times (\sin(2\pi \times freq \times g_{s_1} + \pi) \times \frac{iter_{max} - g_{s_1}}{iter_{max}} + 1) \quad (22)$$

where $freq$ describes a pre-defined frequency for the sinusoidal function and $iter$ denotes the current
 generation number ($g_{s_1} \leq \frac{iter_{max}}{2}$). The second strategy for the adjustment of the scale factor is an
 adaptive sinusoidal adjustment method. This formulation can be seen in Equation 23.

$$F_{i,g} = \frac{1}{2} \times (\sin(2\pi \times freq \times g_{s_1}) \times \frac{g_{s_1}}{iter_{max}} + 1) \quad (23)$$

255 where $freq$ is an adaptive frequency based on a Cauchy distribution and a successful history-based
 256 of settings. $iter$ denotes the current generation number. One of the most effective DE parameter
 257 adaptation techniques is recording an archive of both mutation factors and probabilities of crossover
 258 based on their success during the optimisation process. The control parameters history-based was
 259 proposed by Zhang et al. [64] in JADE. In each generation of JADE, in order to generate an offspring,
 260 we have an array of the crossover probability rate that is produced based on a normal distribution
 261 of the mean (μ_{CR}) and variance at 0.1. The successful crossover probabilities (S_{CR}) are recorded and
 262 updated at each generation. The μ_{CR} is initialised by 0.5 and in the next generation it is updated by
 263 Equation 24.

$$\mu_{CR} = (1 - c) \times \mu_{CR} + c \times \text{mean}_A(S_{CR}) \quad (24)$$

264 where c is a constant generated between 0 and 1 randomly and mean_A is a simple arithmetic mean.
 265 Likewise, the mutation factor F_i of each x_i is separately generated at each generation, as stated in a
 266 Cauchy distribution with the mean μ_F and scale parameter 0.1. (Equation 25)

$$F_i = \text{randc}_i(\mu_F, 0.1) \quad (25)$$

267 where the randc_i is the Cauchy distribution. All successful mutation factors are archived and point out
 268 as a set of S_F at the end of each generation. The value of μ_F is updated using Equation 26.

$$\mu_F = (1 - c) \times \mu_F + c \times \text{mean}_L(S_F) \quad (26)$$

269 where mean_L is the Lehmer mean [65] and computed as follows:

$$\text{mean}_L(S_F) = \frac{\sum_{F \in S_F} F^2}{\sum_{F \in S_F} F} \quad (27)$$

270 Linear Population Size Reduction

271 The LSHADE-EpSin algorithm benefits from a linear reduction in population size to fit the
 272 population size (N) iteratively at each generation as exposed in the following equation:

$$N_{g+1} = \text{Round}\left[\left(\frac{N_{min} - N_{max}}{iter_{max}}\right) \times iter + N_{max}\right] \quad (28)$$

273 where N_{min} is the minimum population size, and initialised at 4 that is required to make the
 274 *current-to-pbest* mutation strategy. The four required solutions are x_i , x_{best}^p , x_{r_1} and x_{r_2} . The mutant
 275 vector of this strategy is generated using Equation 29.

$$V_{i,g} = x_{i,g} + F_i \times (x_{best,g}^p - x_{i,g}) + F_i(x_{r_1,g} - x_{r_2,g}) \quad (29)$$

276 Local Search

277 In order to ~~develop~~ extend the exploitation capability of LSHADE-EpSin, a stochastic local search
 278 is proposed that works based on Gaussian Walks. The local search is activated when the population
 279 size is less than 20 ($N_{ini} = 25$), and 25 random samples are evaluated to exploit the neighbourhood
 280 of the best-found design among the current population. The Gaussian walks applied can be seen in
 281 Equation 30.

$$\mathbf{y}_i = \mathcal{N}(\mu_b, \sigma) + (r_1 \times x_{best} - r_2 \times x_i) \quad (30)$$

282 where x_{best} is the best-found solution in the local search and μ_b is updated by equal to x_{best} . r_1 and r_2
 283 are two uniform random numbers from the range of $[0, 1]$. Besides, the standard deviation (σ) of this
 284 Gaussian Walks is calculated using Equation 31.

$$\sigma = \frac{\log(iter)}{iter} \times (x_i - x_{best}) \quad (31)$$

285 4.2. Bi-Level Optimisation

286 In this paper, we propose two bi-level optimisation methods, including Bi-level-1 (SaDE+NM)
 287 and Bi-level-2 (LSHADE-EpSin+NM). We also provide a general formulation in order to maximise
 288 the harnessed power and minimise the LCoE of a cylindrical wave energy converter. These proposed
 289 approaches comprise two levels of optimisation tasks where one optimisation process is nested within

290 the other. The exterior optimisation method (which is a global search method) is associated with
 291 as referred as the leader's (upper level) optimisation process. In the upper level, we apply two
 292 self-adaptive meta-heuristics, including Self-adaptive DE (SaDE) and LSHADE-EpSin. Both methods
 293 improve the ability of an adaptive learning strategy to fine-tune the control parameters and mutation
 294 strategy and demonstrate a considerable performance in optimising real engineering problems [66,67].

295 In the second level, the internal method is recognised as the follower's (lower level) optimisation
 296 process. In the current study, the inner method is a Nelder-Mead (NM) simplex search method [68].
 297 NM simplex is a downhill local search method, and it is straightforward to hybridise combine with
 298 other meta-heuristic methods. The primary reason for such hybridisation (or for using NM as the
 299 lower-level in a bi-level method) is to tune a more suitable trade-off between global optimality and
 300 computational budgets [69,70].

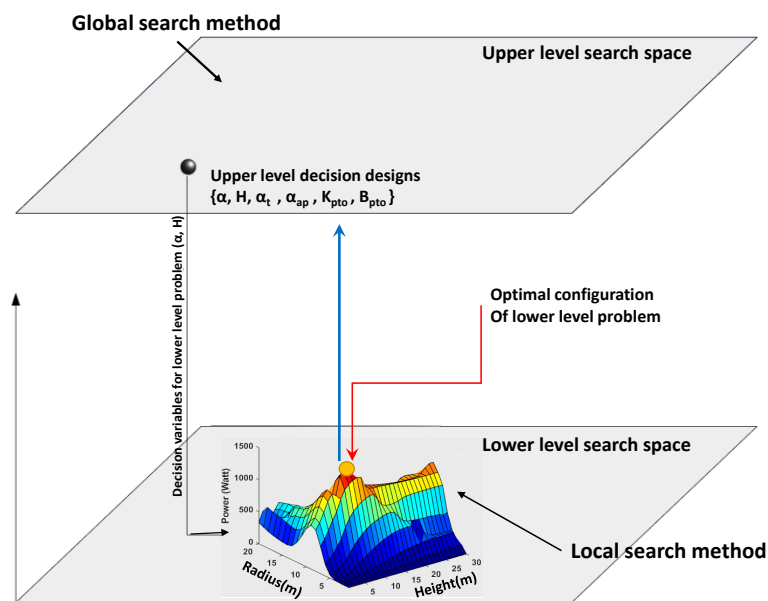


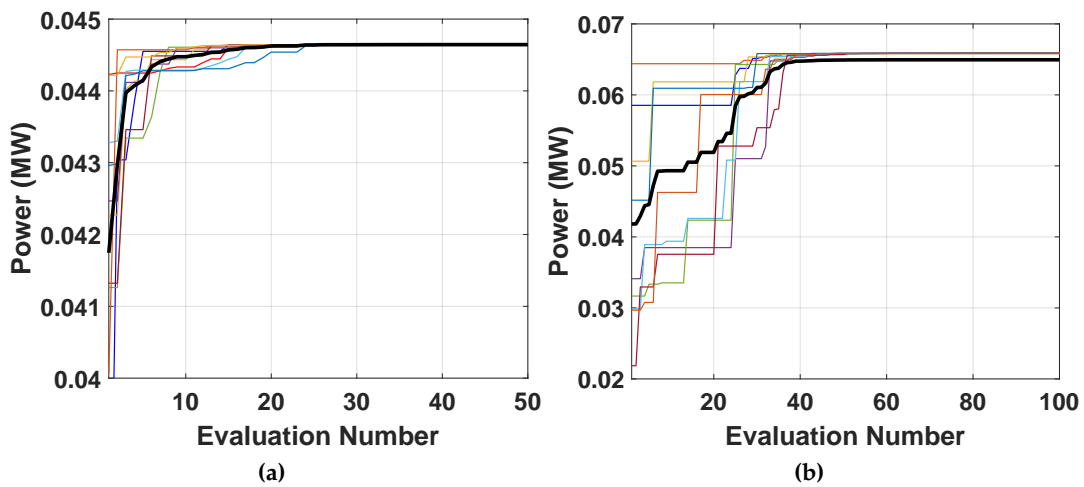
Figure 5. A general sketch of the bi-level optimisation applied in order to maximise the produced power.

301 Figure 5 shows that the proposed bi-level optimisation framework consists of a global search
 302 method designed to optimise all decision variables in the upper-level, and both geometry parameters
 303 (radius and height) that given from upper-level decision vector are optimising in the lower-level. To
 304 adjust the geometry parameters of the cylinder, we use a local search method. The best-found geometry
 305 configuration in the lower-level will be replaced in the upper-level decision variables.

306 The pseudo-code of the proposed Bi-level-2 algorithm is shown in Algorithm 1. It can be seen
 307 that the algorithm is divided into two primary sections. At the top level, we have a self-adaptive DE
 308 (LSHADE-EpSin) employing two strategies to adjust the control parameters. These strategies are (1)
 309 Adaptive sinusoidal increasing adjustment and (2) Non-adaptive sinusoidal decreasing adjustment.
 310 The benefit of this ensemble approach is that it allows the algorithm to converge to a sufficient
 311 balance [36] between searching the neighbourhood of current best-found solutions, and the exploration
 312 of non-visited search space zones. In the lower-level, there are two nested inner local search methods.
 313 The initial local search is used to explore the search space of the cylinder dimensions (radius and
 314 height) where other decision variables are fixed. Next, both tether angles (inclination and attachment)
 315 are optimised using the second local search. In order to save computational budget, we define
 316 a performance criterion for both local search methods. This condition evaluates the local search
 317 performance; if the obtained power improvement cannot satisfy the criterion, Bi-level-2 will withdraw
 318 the local optimisation process and allocate this the remaining budget to the global search method.

319 4.2.1. Tuning the local search

320 One of the significant parameters of the bi-level optimisation method is the maximum evaluation
 321 number (Max_{eval}) of the local search (NM). Tuning this variable plays an important role in obtaining a
 322 greater balance between saving on the computational budget and converging to the local optimum
 323 as much as possible. In order to tune the Max_{eval} , we perform the local search to optimise the WEC
 324 geometry parameters (a, H) and keep the other decision variables fixed. This experiment iterates ten
 325 times with different initial solutions. Meanwhile, the same tuning process runs to optimise both tether
 326 angles. Figure 6 shows the convergence curves of these experiments. We observe that the local search
 327 converges rapidly to a local optimum in the geometry and tether angles optimisation processes after 20
 328 and 40 iterations, respectively on average. Therefore, we set the Max_{eval} of the local search by certain
 tuned values to 20 and 40 iterations.



329 **Figure 6.** The effect of computational budget on tuning the local search iterations. (a) dimension
 330 optimisation (a, H), (b) Tether angles optimisation (α_t, α_{ap}).

330 5. Optimisation results and discussions

331 5.1. Multi-modality of search space

332 In order to characterise the search space, we perform an experiment using a parallel Nelder-Mead
 333 (NM) search method. Twenty random initial configurations are generated and NM is applied to
 334 optimise the absorbed power output. Figure 7 shows the trajectory of the NM performance during
 335 the optimisation process. It can be seen that the majority of the trajectories in the cylinder dimension
 336 (subplot (a)) converged to a specific area of the search space as expected. This is because large WECs
 337 can harness more power than small ones. The second observation is that the PTO search space is not
 338 uni-modal and each trajectory converged to different configurations (subfigure (c,d,e)).

339 5.2. Power landscape analysis

340 With regard to evaluating the impact of each buoy design variable on the level of produced power,
 341 we perform a sensitivity analysis experiment. Here, we assume both tether angles are kept fixed at
 342 45° ; note that this size is not optimal, because tether angles should be adjusted based on the buoy's
 343 dimensions, as recommended by prior works [34]. Moreover, the search space of the K_{pto} and B_{pto}
 344 parameters are discretised, where each interval is 10^6 . In the next step, for each discrete configuration
 345 of PTO parameters, we evaluate the importance of the cylinder dimensions (a, H) using a grid search
 346 technique where the discretisation step size is 1 (m).

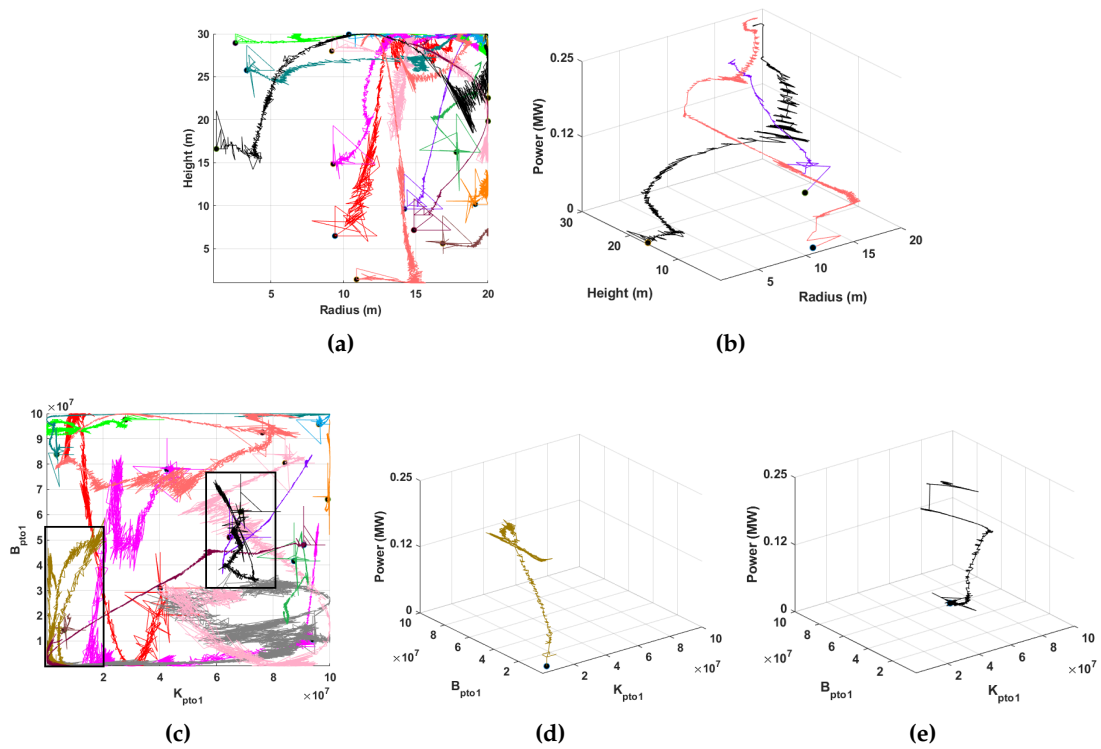


Figure 7. Twenty independent NM runs with the random initial solutions. (a) The NM's trajectory in the cylinder's dimension (radius and height) optimisation, (b) 3D NM's trajectory in the cylinder's dimension and the absorbed power. (c) NM's trajectory in the initial value of the damping (B_{pto}) and spring (K_{pto}) array. (d) and (e) two examples of 3D NM's trajectory in B_{pto} and K_{pto} .

347 The results are shown in Figure 8, which includes 400 sub-figures. Each sub-figure represents the
 348 relationship of the cylinder radius and height sizes with the absorbed power, where the K_{pto} and B_{pto}
 349 are fixed. It is important to note that a variation in the size of the radius has a more substantial effect
 350 on the power output than a variation in the cylinder height. In this wide power landscape, we can
 351 see that the maximum produced powers are achieved when the PTO parameters are assigned around
 352 10^7 , and the buoy radius and height sizes are large. However, it should be noted that the effect of PTO
 353 parameters on the absorbed power is more significant than the size of the cylinder dimensions.

Algorithm 1 Bi-level Optimisation method (LSHADE-EpSin+NM)**procedure** BI-LEVEL OPTIMISATION METHOD**Initialization**

$$P = \{ \langle a_1, H_1, \alpha_{t_1}, \alpha_{ap_1}, K_1^1, \dots, K_1^{10}, B_1^1, \dots, B_1^{10} \rangle, \dots \}$$

$$\dots, \langle a_N, H_N, \alpha_{t_N}, \alpha_{ap_N}, K_N^1, \dots, K_N^{10}, B_N^1, \dots, B_N^{10} \rangle \}$$

▷ initial population

M: $\mu F = \mu CR = 0.5$ ▷ initialise memory of first control settingsM_{freq}: $\mu freq = 0.5, Imp - rate_d = Imp - rate_\alpha = 1$ ▷ initialise memory of second control settings**Upper-Level (Global search method)****for** *iter* in $iter_{max}$ **do** ▷ termination criteria**if** *iter* > $\frac{iter_{max}}{2}$ **then****Call** second control parameter settings $S_F = S_{CR} = \emptyset$ ▷ Reset successful mean vectors $r_i = rand(1, H)$ ▷ Generate a random index, H is memory size $F_i = randc(\mu F_r, 0.1), CR_i = randn(\mu CR_r, 0.1)$ **end if****if** *iter* ≤ $\frac{iter_{max}}{2}$ **then****Call** first control parameter settings $c = rand(0, 1)$ **if** $c < 0.5$ **then**

$$F_i = \frac{1}{2} \times (\sin(2\pi \times freq \times iter + \pi) \times \frac{iter_{max} - iter}{iter_{max}} + 1)$$

else

$$F_i = \frac{1}{2} \times (\sin(2\pi \times freq \times iter) \times \frac{iter}{iter_{max}} + 1)$$

end ifGenerate CR_i same as first control parameters (Equation 23)**end if****for** $i = 1$ to N **do**Generate $p = rand(0, 1) \times n, n = 0.1 \times N$ $v_i = x_i + F_i \times (x_{pbest} - x_i) + F_i \times (x_{r_1} - x_{r_2})$ ▷ Mutation *current-to-pbest* / 1

$$u_{i,iter}^j = \begin{cases} v_{i,iter}^j & \text{if } (rand < CR_i) \text{ or } (j == j_{rand}) \\ P_{i,iter}^j & \text{Otherwise} \end{cases}$$

▷ Binomial Crossover

$$P_{i,iter+1} = \begin{cases} u_{i,iter} & \text{if } (f(u_{i,iter}) > f(P_{i,iter})) \text{ Maximisation} \\ P_{i,iter} & \text{Otherwise} \end{cases}$$

▷ Selection

Store successful F_i and CR_i **end for**

Update the memory according to used settings

Update the population size by Equation 28

$$N_{diff} = N_g - N_{g+1}$$

Sort P_{iter} based on the fitness functionRemove worst solutions N_{diff} from P_{iter} AND Select the best solution P_{best} **Lower-Level (Local search method)****if** $Imp - rate_d > 0.001\%$ **then** ▷ Optimise Cylinder dimension

$$P_{best}(a, H) = Nelder - Mead(P_{best}(a, H), Max_{eval})$$

Compute improvement rate $Imp - rate_d$ **end if****if** $Imp - rate_\alpha > 0.001\%$ **then** ▷ Optimise tether angles

$$P_{best}(\alpha_t, \alpha_{ap}) = Nelder - Mead(P_{best}(\alpha_t, \alpha_{ap}), Max_{eval})$$

Compute improvement rate $Imp - rate_\alpha$ **end if**Update P_{iter}^{best} by the best-found NM configurations**end for****end procedure**

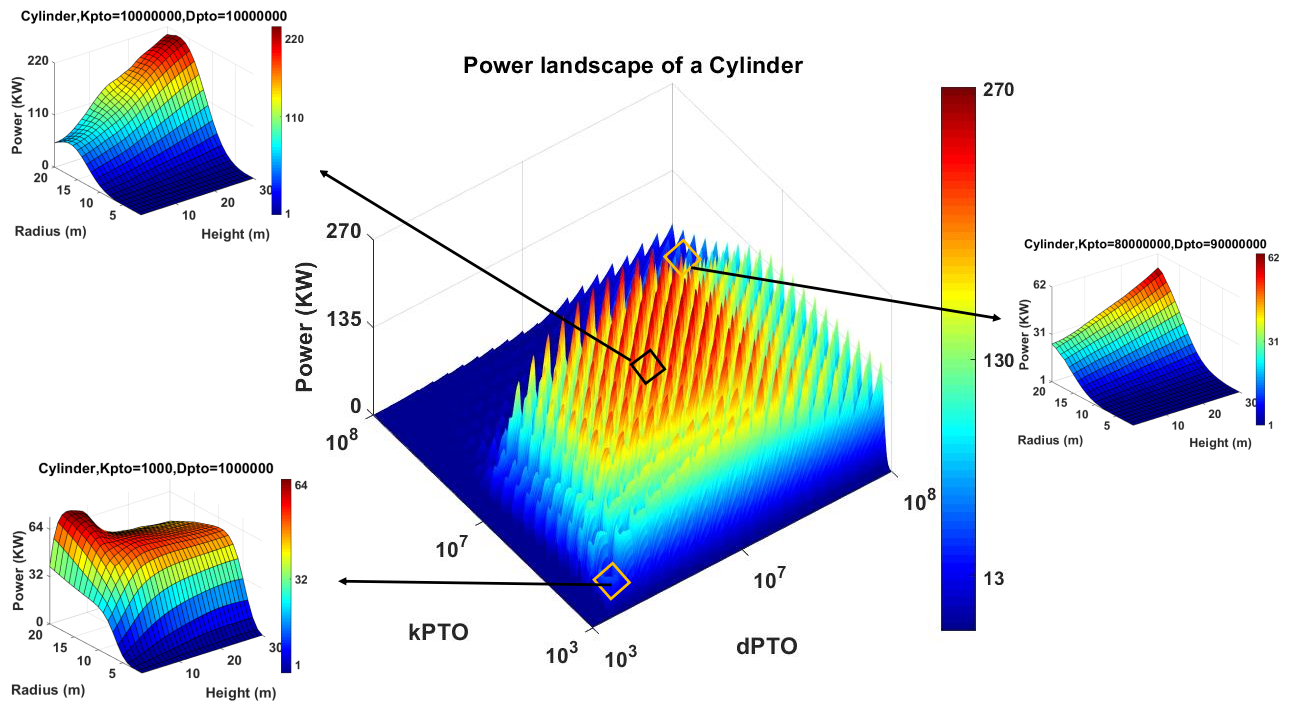


Figure 8. A power landscape of the cylinder with the fixed angles $\alpha_t, \alpha_{ap} = 45$ and various dimensions and PTO parameters

355 5.3. The annual average power output maximisation

356 In this section, we describe the optimisation results of our cylinder design experiments in order
 357 to maximise the annual average power output. Furthermore, we compare the performance of the
 358 optimisation algorithms outlined above in terms of best-found designs and speed of convergence.

359 Table 4 reports the best-found cylinder designs using seven meta-heuristics and two new bi-level
 360 optimisation methods that produced the highest power output among all ten runs. Furthermore, it
 361 can be seen that Bi-level-2 performs better than other applied optimisation methods and that it can
 362 produce a considerable amount of power of 279 kW. The second observation is that almost all (8 out of
 363 9) optimisation methods converged to the cylinder of 15 m radius with the largest possible height of 30
 364 m. However, it should be noted that producing electricity using such large WECs can be expensive,
 365 due to the high manufacturing costs. In terms of the angles and PTO settings, a large range of values is
 366 proposed by all optimisation methods even though the maximised power output is not dramatically
 367 different. This fact proves that it is not straightforward to optimise a multi-mode WEC due to the
 368 strong dependencies between angles, PTO parameters, and the hydrodynamic model which dominates
 369 the power absorption (heave, surge or pitch).

Table 4. Best-found design parameters in order to maximise the average annual absorbed power.

Parameter	1+1EA	CMA-ES	PSO	GWO	DE	SaDE	LSHADE-EpSin	Bi-Level-1	Bi-Level-2
a [m]	16.62	16.10	19.99	16.68	15.46	15.50	15.49	15.61	14.51
H [m]	30	30	14.80	30	30	30	30	30	30
α_t [deg]	70	26	60	14	48	26	39	50	10
α_{ap} [deg]	10	13	63	28	10	11	29	40	67
$\sum_{i=1}^{N_K} K_{pto} (\times 10^7)$	0.665	0.863	3.796	1.51	1.894	2.883	0.882	0.665	0.514
$\sum_{i=1}^{N_B} B_{pto} (\times 10^7)$	2.765	3.928	4.676	1.51	3.775	4.036	2.479	2.095	1.129
P_{AAP} [kW]	259	248	239	261	259	261	262	265	279

370 Table 6 presents the average best-found power output per each run for all optimisation methods.
 371 Bi-level-2 is not only capable of finding the best design configuration; it also performs the best average
 372 power output (Figure 9(a)) compared with other meta-heuristics. In terms of the convergence rate,
 373 Figure 10(a) depicts the applied optimisation method experiments during the 5000 evaluations. As
 374 we can see, GWO and LSHADE-SeSin rapidly converge to considerable settings; however, they could
 375 not sustain this upward trajectory and converge near locally optimal designs. Obviously, the fastest
 376 convergence rate is allocated to Bi-level-2.

377 5.4. LCoE minimisation

378 In this section, we describe the second applied objective function related to LCoE and
 379 approximated as a ratio of the generated energy to the significant mass of the system. The best-found
 380 LCoE values and their relevant cylinder configurations which are obtained using nine meta-heuristic
 381 approaches are shown in Table 5. Interestingly, all optimisation methods (except PSO) converged
 382 to a narrow range of radii between 5 and 7.3 m, with the smallest possible aspect ratio of 0.4. This
 383 geometry leads to the fact that the power generation will be dominated by the heave mode rather than
 384 surge. Moreover, this is clearly seen from the optimised values of the tether angles as to absorb power
 385 from the vertical motion, the tether angles should be closer to vertical leading to $\alpha_t < 35^\circ$. Another
 386 important finding is that the power production of WECs optimised for LCoE is relatively low leading
 387 to 28.3 kW.

388 Figure 9(b) shows the box-and-whiskers plot for the best configurations of the WEC which deliver
 389 the minimum LCoE for each run for nine search heuristics. It can be seen that the performance
 390 of Bi-level-2 is more reliable than that of the other meta-heuristic algorithms we applied. Both
 391 LSHADE-EpSin and Bi-level-1 show the next best average performances by 0.028 and 0.0295,
 392 respectively.

393 Investigating the convergence trajectories (Figure 10) from this experiment in the real wave model,
 394 it is clear that Bi-level-2 converges faster than other optimisation methods. It is noteworthy that among
 395 the seven optimisation methods in the all-at-once strategy, the LSHADE-EpSin convergence speed is
 396 substantially better than the others due to both adaptive and non-adaptive strategies in order to adjust
 397 the control parameters as well as to conduct an embedded local search in the initial iterations. However,
 398 it can be seen that the convergence rate of GWO is considerable in the initial 1000 evaluations.

399 In order to see the convergence performance of Bi-level optimisation algorithms, the search
 400 trajectory of the best agent in each generation for all decision variables is shown in Figure 11. Initially,
 401 we can see the high convergence ability of Bi-level-2 compared with DE in order to find and converge
 402 to the optimal range of both radius and height. Meanwhile, It can be observed that Bi-level-2 tends to
 explore promising areas of the tether angle search space broadly, and finally, to exploit the best values.

Table 5. Best-found design parameters in order to minimise the LCoE.

Parameter	1+1EA	CMA-ES	PSO	GWO	DE	SaDE	LSHADE-EpSin	Bi-Level-1	Bi-Level-2
a [m]	7.31	6.40	14.32	7.00	7.38	6.57	5.00	6.15	5.00
H/a	0.40	0.40	0.40	0.4	0.40	0.40	0.40	0.40	0.40
α_t [deg]	28	29	10	10	31	25	35	31	34
α_{ap} [deg]	10	11	10	31	14	11	10	12	10
$\sum_{i=1}^{N_k} K_{pto} (\times 10^7)$	0.647	0.919	3.90	0.651	3.50	0.383	2.094	0.77	2.071
$\sum_{i=1}^{N_B} B_{pto} (\times 10^7)$	0.577	0.332	3.52	0.847	1.15	0.481	1.350	0.256	1.914
LCoE	0.0316	0.0284	0.0556	0.0297	0.0287	0.0277	0.0248	0.0267	0.0243
P_{AAP} [kW]	53.1	43.6	131	51.4	64.8	50.6	27.1	43.5	28.3

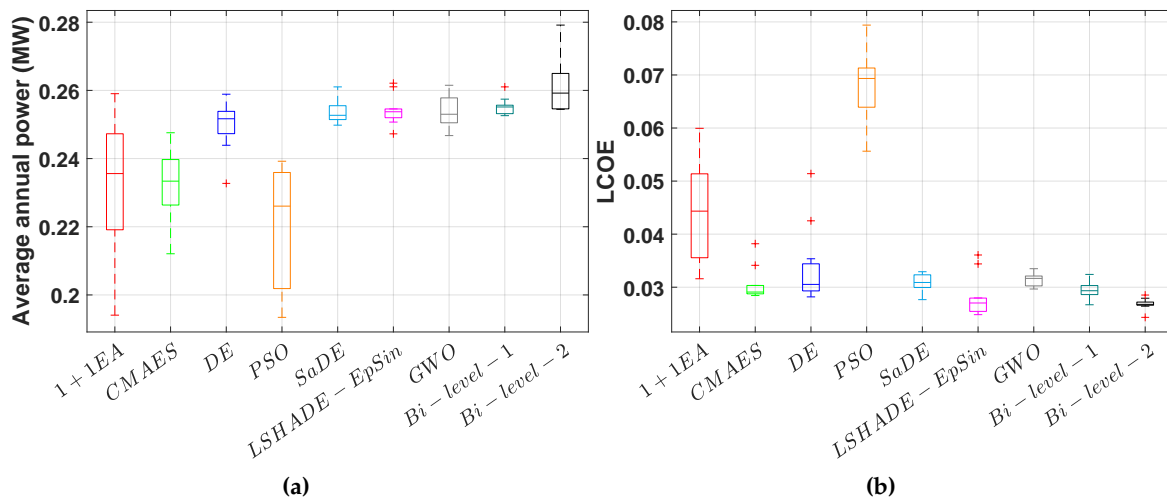
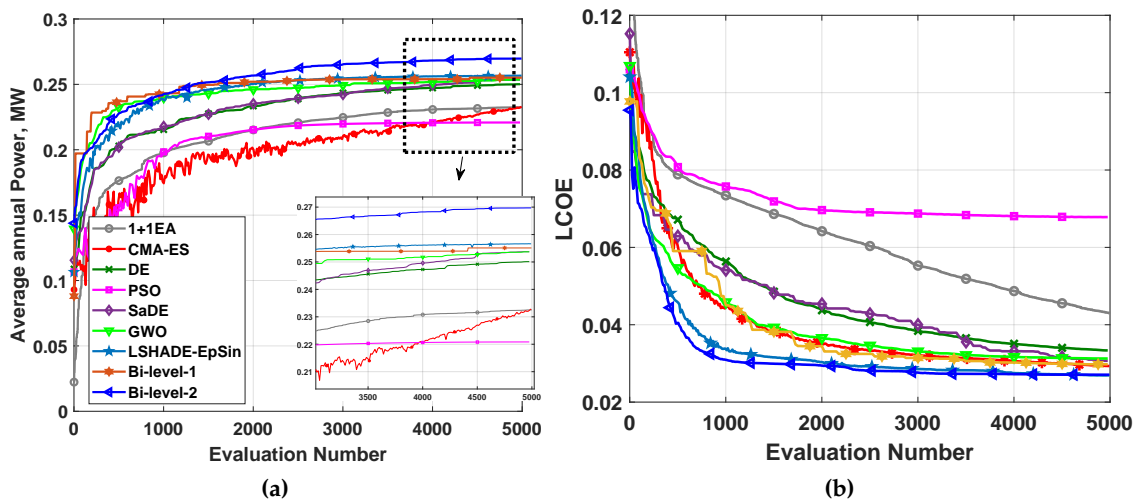
403

404 6. Conclusions

405 In this paper, two new bi-level optimisation methods are proposed with the aim of maximising the
 406 harnessed power output. These methods are also designed to minimise the levelised cost of energy of

Table 6. Performance comparison of various optimisation methods based on the maximum, minimum and average power output and LCoE of the best-found design per each experiment.

		Power [MW]								
	1+1EA	CMA-ES	PSO	GWO	DE	SaDE	LSHADE-EpSin	Bi-Level-1	Bi-Level-2	
Mean	0.2325	0.2329	0.2208	0.2537	0.2501	0.2537	0.2541	0.2551	0.2612	
Min	0.1941	0.2121	0.1934	0.2467	0.2327	0.2498	0.2473	0.2526	0.2544	
Max	0.2590	0.2476	0.2392	0.2615	0.2589	0.2610	0.2621	0.2610	0.2792	
STD	0.0234	0.0117	0.0181	0.0049	0.0087	0.0036	0.0046	0.0032	0.0088	
		LCoE								
	1+1EA	CMA-ES	PSO	GWO	DE	SaDE	LSHADE-EpSin	Bi-Level-1	Bi-Level-2	
Mean	0.0443	0.0303	0.0678	0.0315	0.0334	0.0309	0.0280	0.0295	0.0268	
Min	0.0316	0.0284	0.0556	0.0297	0.0282	0.0277	0.0248	0.0267	0.0243	
Max	0.0599	0.0382	0.0794	0.0335	0.0514	0.0329	0.0361	0.0324	0.0285	
STD	0.0109	0.0036	0.0071	0.0014	0.0079	0.0019	0.0041	0.0019	0.0012	

**Figure 9.** Each method runs 10 times. (a) Average annual produced power, (b) Levelised cost of energy (LCoE).**Figure 10.** The average convergence rate comparison of the absorbed power and LCoE of the Cylinder. Each method runs 10 times. (a) Average annual produced power, (b) Levelised cost of energy (LCoE).

407 a fully-submerged, cylindrical WEC with three tethers for the wave climate of a Mediterranean sea site
 408 in the west of Sicily, Italy (featuring unidirectional irregular waves). The optimisation of a combination
 409 of WEC radius, height, tether inclination and attachment angles, and power take-off parameters is a

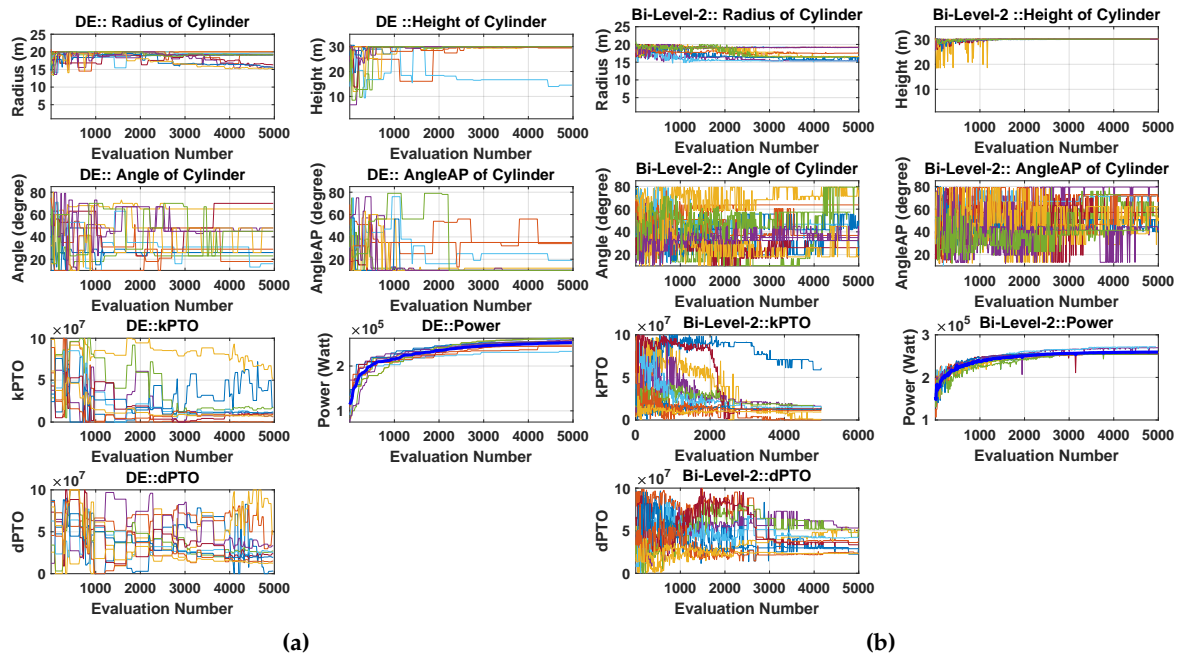


Figure 11. Search history and trajectory of the best solution per each population in the all decision variables. a) the optimisation process (power maximisation) of DE, b) Bi-level-2

410 relatively computationally expensive (5000 evaluations take around 15 hours), multi-modal, large-scale
 411 and complex problem. These characteristics provided the principal motivation for investigating
 412 and proposing a faster and more reliable optimisation technique. With this in mind, we applied
 413 a bi-level strategy to optimise the design variables at various levels. A global search method was
 414 used at the upper level to optimise the parameters of the whole WEC's. Furthermore, in the lower
 415 level, a Nelder-Mead (NM) simplex search method was applied to adjust the geometry settings and
 416 tether angles. To systematically compare the effectiveness of the proposed optimisation method,
 417 we considered seven state-of-the-art evolutionary and swarm algorithms. The experimental results
 418 showed that the bi-level method can outperform other meta-heuristics in terms of both convergence
 419 rate and the quality of WEC's configuration. Moreover, according to the best-found configurations, if
 420 we focus on maximising the harnessed power output without considering the costs, a large cylindrical
 421 buoy is recommended. However, the cheapest energy can be delivered by a relatively small WEC with
 422 a radius of 5 m and a height of 2 m.

423 **Acknowledgments:** The authors would like to express their gratitude to Civil Engineering Department of
 424 Catania University and Favignana Municipality for their cooperation to provide all data. This research has been
 425 carried out within ODYSSEA project that received funding from the European Union's Horizon 2020 research and
 426 innovation programme under grant agreement No 727277. Moreover, we would like to show our gratitude to Dr.
 427 Fabien Voisin from the information technology and digital services, the University of Adelaide due to his valuable
 428 participation in the parallel computing services. This research is supported by the supercomputing resources
 429 provided by the Phoenix HPC service at the University of Adelaide.

430 **Funding:** This research was funded by European Union's Horizon 2020 research and innovation programme
 431 under grant agreement No 727277 within the project ODYSSEA "Operating a network of integrated observatory
 432 systems in the Mediterranean sea" in order to collect data.

433 **Conflicts of Interest:** The authors declare no conflict of interest.

434 Abbreviations

435 The following abbreviations are used in this manuscript:

436

WEC	Wave Energy Converter
PTO	Power Take-off system
PSO	Particle Swarm Optimisation
437 DE	Differential Evolution
SaDE	Self adaptive Differential Evolution
CMA-ES	Covariance Matrix Adaptation Evolution Strategy
LSHADE	Local Success-history Adaptive Differential Evolution

438

- 439 1. Murdock, H.E.; Gibb, D.; André, T.; Appavou, F.; Brown, A.; Epp, B.; Kondev, B.; McCrone, A.; Musolino,
440 E.; Ranalder, L.; others. Renewables 2019 global status report **2019**.
- 441 2. Tronchin, L.; Manfren, M.; Nastasi, B. Energy analytics for supporting built environment decarbonisation.
442 *Energy Procedia* **2019**, *157*, 1486–1493.
- 443 3. Mazzoni, S.; Ooi, S.; Nastasi, B.; Romagnoli, A. Energy storage technologies as techno-economic parameters
444 for master-planning and optimal dispatch in smart multi energy systems. *Applied Energy* **2019**, *254*, 113682.
- 445 4. Aderinto, T.; Li, H. Ocean wave energy converters: Status and challenges. *Energies* **2018**, *11*, 1250.
- 446 5. Falnes, J. A review of wave-energy extraction. *Marine structures* **2007**, *20*, 185–201.
- 447 6. Astariz, S.; Iglesias, G. Wave energy vs. other energy sources: A reassessment of the economics. *International*
448 *Journal of Green Energy* **2016**, *13*, 747–755.
- 449 7. Wen, Y.; Wang, W.; Liu, H.; Mao, L.; Mi, H.; Wang, W.; Zhang, G. A Shape Optimization Method of a
450 Specified Point Absorber Wave Energy Converter for the South China Sea. *Energies* **2018**, *11*, 2645.
- 451 8. Alamian, R.; Shafaghat, R.; Safaei, M.R. Multi-Objective Optimization of a Pitch Point Absorber Wave
452 Energy Converter. *Water* **2019**, *11*, 969.
- 453 9. Esmaeilzadeh, S.; Alam, M.R. Shape optimization of wave energy converters for broadband directional
454 incident waves. *Ocean Engineering* **2019**, *174*, 186–200. doi:<https://doi.org/10.1016/j.oceaneng.2019.01.029>.
- 455 10. Wang, L.; Ringwood, J.V. Geometric optimization of a hinge-barge wave energy converter. Proceedings of
456 the 13th European Wave and Tidal Energy Conference, 2019, p. 1389.
- 457 11. Garcia-Teruel, A.; Forehand, D.I.M.; Jeffrey, H. Metrics for wave energy converter hull geometry
458 optimisation. Proceedings of the 13th European Wave and Tidal Energy Conference. EWTEC, 2019.
- 459 12. Sergiienko, N.Y.; Neshat, M.; da Silva, L.S.; Alexander, B.; Wagner, M. Design optimisation of a multi-mode
460 wave energy converter. Proceedings of ASME 2020 39th International Conference on Ocean, Offshore and
461 Arctic Engineering (OMAE2020). ASME, 2020.
- 462 13. Abdelkhalik, O.; Zou, S.; Robinett, R.D.; Bacelli, G.; Wilson, D.; Coe, R.G.; Korde, U.A. Multiresonant
463 Feedback Control of a Three-Degree-of-Freedom Wave Energy Converter. *IEEE Transactions on Sustainable*
464 *Energy* **2017**, *8*, 1518–1527.
- 465 14. Neshat, M.; Alexander, B.; Sergiienko, N.; Wagner, M. A Hybrid Evolutionary Algorithm Framework for
466 Optimising Power Take Off and Placements of Wave Energy Converters. *arXiv preprint arXiv:1904.07043*
467 **2019**.
- 468 15. Sharp, C.; DuPont, B. Wave energy converter array optimization: A genetic algorithm approach and
469 minimum separation distance study. *Ocean Engineering* **2018**, *163*, 148–156.
- 470 16. Fang, H.W.; Feng, Y.Z.; Li, G.P. Optimization of Wave Energy Converter Arrays by an Improved Differential
471 Evolution Algorithm. *Energies* **2018**, *11*, 3522.
- 472 17. Neshat, M.; Alexander, B.; Wagner, M.; Xia, Y. A detailed comparison of meta-heuristic methods for
473 optimising wave energy converter placements. Proceedings of the Genetic and Evolutionary Computation
474 Conference. ACM, 2018, pp. 1318–1325.
- 475 18. Neshat, M.; Alexander, B.; Sergiienko, N.Y.; Wagner, M. Optimisation of Large Wave Farms Using a
476 Multi-Strategy Evolutionary Framework. Proceedings of the 2020 Genetic and Evolutionary Computation
477 Conference; Association for Computing Machinery: New York, NY, USA, 2020; GECCO '20, p. 1150–1158.
478 doi:10.1145/3377930.3390235.
- 479 19. Giassi, M.; Castellucci, V.; Göteman, M. Economical layout optimization of wave energy parks clustered in
480 electrical subsystems. *Applied Ocean Research* **2020**, *101*, 102274. doi:10.1016/j.apor.2020.102274.

- 481 20. Fairley, I.; Lewis, M.; Robertson, B.; Hemer, M.; Masters, I.; Horrillo-Caraballo, J.; Karunarathna, H.; Reeve,
482 D.E. A classification system for global wave energy resources based on multivariate clustering. *Applied*
483 *Energy* **2020**, *262*, 114515.
- 484 21. Franzitta, V.; Rizzo, G. Renewable energy sources: A mediterranean perspective. 2010 2nd International
485 Conference on Chemical, Biological and Environmental Engineering. IEEE, 2010, pp. 48–51.
- 486 22. Rusu, E.; Onea, F. Estimation of the wave energy conversion efficiency in the Atlantic Ocean close to the
487 European islands. *Renewable Energy* **2016**, *85*, 687–703.
- 488 23. Rusu, E. Wave energy assessments in the Black Sea. *Journal of marine science and technology* **2009**, *14*, 359–372.
- 489 24. Bouali, B.; Larbi, S. Contribution to the geometry optimization of an oscillating water column wave energy
490 converter. *Energy procedia* **2013**, *36*, 565–573.
- 491 25. Kramer, M.V.; Frigaard, P.; others. Efficient wave energy amplification with wave reflectors. The Twelfth
492 International Offshore and Polar Engineering Conference. International Society of Offshore and Polar
493 Engineers, 2002.
- 494 26. Vantorre, M.; Banasiak, R.; Verhoeven, R. Modelling of hydraulic performance and wave energy extraction
495 by a point absorber in heave. *Applied Ocean Research* **2004**, *26*, 61–72.
- 496 27. Goggins, J.; Finnegan, W. Shape optimisation of floating wave energy converters for a specified wave
497 energy spectrum. *Renewable Energy* **2014**, *71*, 208–220.
- 498 28. Hager, R.; Fernandez, N.; Teng, M.H.; others. Experimental study seeking optimal geometry of a heaving
499 body for improved power absorption efficiency. The Twenty-second International Offshore and Polar
500 Engineering Conference. International Society of Offshore and Polar Engineers, 2012.
- 501 29. McCabe, A. Constrained optimization of the shape of a wave energy collector by genetic algorithm.
502 *Renewable energy* **2013**, *51*, 274–284.
- 503 30. de Andres, A.; MacGillivray, A.; Roberts, O.; Guancho, R.; Jeffrey, H. Beyond LCOE: A study of ocean
504 energy technology development and deployment attractiveness. *Sustainable Energy Technologies and*
505 *Assessments* **2017**, *19*, 1–16.
- 506 31. Piscopo, V.; Benassai, G.; Della Morte, R.; Scamardella, A. Cost-based design and selection of point absorber
507 devices for the mediterranean sea. *Energies* **2018**, *11*, 946.
- 508 32. Piscopo, V.; Benassai, G.; Cozzolino, L.; Della Morte, R.; Scamardella, A. A new optimization procedure of
509 heaving point absorber hydrodynamic performances. *Ocean Engineering* **2016**, *116*, 242–259.
- 510 33. Piscopo, V.; Benassai, G.; Della Morte, R.; Scamardella, A. Towards a cost-based design of heaving point
511 absorbers. *International journal of marine energy* **2017**, *18*, 15–29.
- 512 34. Sergiienko, N.Y.; Cazzolato, B.S.; Ding, B.; Arjomandi, M. An optimal arrangement of mooring lines for
513 the three-tether submerged point-absorbing wave energy converter. *Renewable Energy* **2016**, *93*, 27–37.
514 doi:<http://dx.doi.org/10.1016/j.renene.2016.02.048>.
- 515 35. Mirjalili, S.; Mirjalili, S.M.; Lewis, A. Grey wolf optimizer. *Advances in engineering software* **2014**, *69*, 46–61.
- 516 36. Awad, N.H.; Ali, M.Z.; Suganthan, P.N.; Reynolds, R.G. An ensemble sinusoidal parameter adaptation
517 incorporated with L-SHADE for solving CEC2014 benchmark problems. 2016 IEEE congress on
518 evolutionary computation (CEC). IEEE, 2016, pp. 2958–2965.
- 519 37. Iuppa, C.; Cavallaro, L.; Vicinanza, D.; Foti, E. Investigation of suitable sites for Wave Energy Converters
520 around Sicily (Italy). *Ocean Science Discussions* **2015**, *12*.
- 521 38. Silva, L.; Sergiienko, N.; Pesce, C.; Ding, B.; Cazzolato, B.; Morishita, H. Stochastic analysis of
522 nonlinear wave energy converters via statistical linearization. *Applied Ocean Research* **2020**, *95*, 102023.
523 doi:<https://doi.org/10.1016/j.apor.2019.102023>.
- 524 39. Silva, L.S.P. Nonlinear stochastic analysis of wave energy converters via statistical linearization. MSc
525 thesis, University of São Paulo, Brazil, 2019.
- 526 40. Folley, M. *Numerical modelling of wave energy converters: State-of-the-art techniques for single devices and arrays*;
527 Elsevier Science: Saint Louis, 2016.
- 528 41. Spanos, P.D.; Arena, F.; Richichi, A.; Malara, G. Efficient dynamic analysis of a nonlinear wave energy
529 harvester model. *Journal of Offshore Mechanics and Arctic Engineering* **2016**, *138*, 041901.
- 530 42. Silva, L.S.P.; Morishita, H.M.; Pesce, C.P.; Gonçalves, R.T. Nonlinear analysis of a heaving point absorber
531 in frequency domain via statistical linearization. ASME 2019 38th International Conference on Ocean,
532 Offshore and Arctic Engineering. American Society of Mechanical Engineers, 2019.

- 533 43. Penalba, M.; Giorgi, G.; Ringwood, J.V. Mathematical modelling of wave energy converters: A review of
534 nonlinear approaches. *Renewable and Sustainable Energy Reviews* **2017**, *78*, 1188–1207.
- 535 44. Scruggs, J.T.; Lattanzio, S.M.; Taflanidis, A.A.; Cassidy, I.L. Optimal causal control of
536 a wave energy converter in a random sea. *Applied Ocean Research* **2013**, *42*, 1–15.
537 doi:http://dx.doi.org/10.1016/j.apor.2013.03.004.
- 538 45. da Silva, L.S.P.; Cazzolato, B.S.; Sergiienko, N.Y.; Ding, B.; Morishita, H.M.; Pesce, C.P. Statistical
539 linearization of the Morison's equation applied to wave energy converters. *Journal of Ocean Engineering and
540 Marine Energy* **2020**, pp. 1–13.
- 541 46. De Andres, A.; Maillet, J.; Hals Todalshaug, J.; Möller, P.; Bould, D.; Jeffrey, H. Techno-Economic Related
542 Metrics for a Wave Energy Converters Feasibility Assessment. *Sustainability* **2016**, *8*, 1109.
- 543 47. Sergiienko, N.Y.; Rafiee, A.; Cazzolato, B.S.; Ding, B.; Arjomandi, M. Feasibility study of
544 the three-tether axisymmetric wave energy converter. *Ocean Engineering* **2018**, *150*, 221–233.
545 doi:https://doi.org/10.1016/j.oceaneng.2017.12.055.
- 546 48. Jiang, S.C.; Gou, Y.; Teng, B. Water wave radiation problem by a submerged cylinder. *Journal of Engineering
547 Mechanics* **2014**, *140*, 6014003. doi:10.1061/(ASCE)EM.1943-7889.0000723.
- 548 49. Jiang, S.C.; Gou, Y.; Teng, B.; Ning, D.Z. Analytical solution of a wave diffraction problem on a submerged
549 cylinder. *Journal of Engineering Mechanics* **2014**, *140*, 225–232. doi:10.1061/(ASCE)EM.1943-7889.0000637.
- 550 50. Hoerner, S. *Fluid-dynamic drag: Practical information on aerodynamic drag and hydrodynamic resistance*; Hoerner
551 Fluid Dynamics, 1965.
- 552 51. The Specialist Committee on Waves. Final Report and Recommendations to the 23rd ITTC. Proceedings of
553 the 23rd International Towing Tank Conference, 2002, Vol. II, pp. 505–736.
- 554 52. Sinha, A.; Malo, P.; Deb, K. A review on bilevel optimization: from classical to evolutionary approaches
555 and applications. *IEEE Transactions on Evolutionary Computation* **2017**, *22*, 276–295.
- 556 53. McKinnon, K.I. Convergence of the Nelder–Mead Simplex Method to a Nonstationary Point. *SIAM Journal
557 on optimization* **1998**, *9*, 148–158.
- 558 54. Jansen, T.; Wegener, I. On the choice of the mutation probability for the (1+ 1) EA. International Conference
559 on Parallel Problem Solving from Nature. Springer, 2000, pp. 89–98.
- 560 55. Hansen, N. The CMA evolution strategy: a comparing review. *Towards a new evolutionary computation* **2006**,
561 pp. 75–102.
- 562 56. Eberhart, R.; Kennedy, J. A new optimizer using particle swarm theory. Symposium on Micro Machine
563 and Human Science (MHS). IEEE, 1995, pp. 39–43.
- 564 57. Storn, R.; Price, K. Differential evolution—a simple and efficient heuristic for global optimization over
565 continuous spaces. *Journal of global optimization* **1997**, *11*, 341–359.
- 566 58. Qin, A.K.; Huang, V.L.; Suganthan, P.N. Differential evolution algorithm with strategy adaptation for
567 global numerical optimization. *IEEE transactions on Evolutionary Computation* **2008**, *13*, 398–417.
- 568 59. Neumann, F.; Wegener, I. Randomized local search, evolutionary algorithms, and the minimum spanning
569 tree problem. *Theoretical Computer Science* **2007**, *378*, 32–40.
- 570 60. Goudos, S.K.; Deruyck, M.; Plets, D.; Martens, L.; Joseph, W. Optimization of power consumption in 4G
571 LTE networks using a novel barebones self-adaptive differential evolution algorithm. *Telecommunication
572 Systems* **2017**, *66*, 109–120.
- 573 61. Ramli, M.A.; Bouchekara, H.; Alghamdi, A.S. Optimal sizing of PV/wind/diesel hybrid microgrid system
574 using multi-objective self-adaptive differential evolution algorithm. *Renewable energy* **2018**, *121*, 400–411.
- 575 62. Tanabe, R.; Fukunaga, A.S. Improving the search performance of SHADE using linear population size
576 reduction. 2014 IEEE congress on evolutionary computation (CEC). IEEE, 2014, pp. 1658–1665.
- 577 63. Tanabe, R.; Fukunaga, A. Success-history based parameter adaptation for differential evolution. 2013 IEEE
578 congress on evolutionary computation. IEEE, 2013, pp. 71–78.
- 579 64. Zhang, J.; Sanderson, A.C. JADE: adaptive differential evolution with optional external archive. *IEEE
580 Transactions on evolutionary computation* **2009**, *13*, 945–958.
- 581 65. Bullen, P.S. *Handbook of means and their inequalities*; Vol. 560, Springer Science & Business Media, 2013.
- 582 66. Goudos, S.K.; Siakavara, K.; Samaras, T.; Vafiadis, E.E.; Sahalos, J.N. Self-adaptive differential evolution
583 applied to real-valued antenna and microwave design problems. *IEEE Transactions on Antennas and
584 Propagation* **2011**, *59*, 1286–1298.

- 585 67. Rajagopalan, A.; Sengoden, V.; Govindasamy, R. Solving economic load dispatch problems using chaotic
586 self-adaptive differential harmony search algorithm. *International Transactions on Electrical Energy Systems*
587 **2015**, *25*, 845–858.
- 588 68. Nelder, J.A.; Mead, R. A simplex method for function minimization. *The computer journal* **1965**, *7*, 308–313.
- 589 69. Ghasemi, M.; Ghavidel, S.; Ghanbarian, M.M.; Habibi, A. A new hybrid algorithm for optimal reactive
590 power dispatch problem with discrete and continuous control variables. *Applied soft computing* **2014**,
591 *22*, 126–140.
- 592 70. Rajan, A.; Malakar, T. Optimal reactive power dispatch using hybrid Nelder–Mead simplex based firefly
593 algorithm. *International Journal of Electrical Power & Energy Systems* **2015**, *66*, 9–24.

594 © 2021 by the authors. Submitted to *Journal Not Specified* for possible open access
595 publication under the terms and conditions of the Creative Commons Attribution (CC BY) license
596 (<http://creativecommons.org/licenses/by/4.0/>).